Available online at www.sciencedirect.com

ScienceDirect

journal homepage: www.elsevier.com/locate/he

Hydriding and dehydriding in air-exposed Mg–Fe powder mixtures

K. Suárez-Alcántara [a,*], A.F. Palacios-Lazcano [b], T. Funatsu [c], J.G. Cabañas-Moreno [d]

[a] Unidad Morelia del Instituto de Investigaciones en Materiales de la Universidad Nacional Autónoma de México, Antigua carretera a Pátzcuaro 8701, Col. Ex-hacienda de San José de la Huerta, Morelia, Michoacán, 58190, Mexico
[b] ESIME Zacatenco, Av. Luis Enrique Erro S/N, Unidad Profesional Adolfo López Mateos, Zacatenco, Delegación Gustavo A. Madero, Distrito Federal, 07738, Mexico
[c] Techno System Co., Ltd, Karasakinaka 3-1-1, Takatsuki-City, Osaka, Japan
[d] Centro de Investigación y de Estudios Avanzados, IPN, Av. Instituto Politécnico Nacional 2508, México, D. F., 07360, Mexico

ARTICLE INFO

Article history:
Received 25 February 2016
Received in revised form
29 June 2016
Accepted 29 June 2016
Available online 14 July 2016

Keywords:
Hydrogen storage
Air exposed Mg–Fe mixtures
Activation of Mg

ABSTRACT

Mg–Fe mixtures, with a nominal Fe content of 3 wt.% and 6 wt.%, hereafter Mg–Fe (3 wt.%) and Mg–Fe (6 wt.%), were produced by ball milling and exposed to air for 12 h. After a proper activation procedure, which consisted in heating in vacuum and three hydriding/dehydriding cycles; their hydriding and dehydriding reactions were characterized by a gravimetric method. The hydrogen uptakes were 5.3 wt. %, 5.6 wt. % and 6.2 wt. % for the air-exposed Mg, Mg–Fe (3 wt.%) and Mg–Fe (6 wt.%) mixtures respectively at 350 °C and 30 bar. Pressure-Composition-Temperature (PCT) curves demonstrated a reduction of the hysteresis of the Mg–Fe mixtures as compared to pure Mg. Powder X-ray diffraction of the studied materials confirmed the formation of fine mixtures of Mg and Fe, without evidence of solid solution or mixed hydride formation.

Introduction

Hydrogen is a promising alternative to fossil fuels; however for tangible applications, it is necessary to develop the "perfect" hydrogen storage material and the corresponding large-scale production systems. On the road for that "perfect" hydrogen storage material, Mg/MgH_2 and its alloys had been extensively studied [1–4]. It is agreed that Mg/MgH_2 is not suitable for mobile applications due to its high dehydriding temperature, relatively slow hydriding/dehydriding kinetics, and insufficient energy storage density. However, niche applications, where neither the working temperature nor weight/volume restrictions applies or where a low-cost material is needed, are still possible. Heat storage or hydrogen storage for stationary applications are some examples of such possible applications [5].

Fe had been reported as a suitable additive for improving hydriding/dehydriding kinetics in several systems. Some outstanding examples include: i) the addition of Fe to Mg/MgH_2 in several concentrations, from fractions of mole up to

* *Corresponding author*. Universidad Nacional Autónoma de México, Instituto de Investigación en Materiales sede Morelia, Antigua Carretera a Pátzcuaro No. 8701, Col. Ex Hacienda de San José de la Huerta C.P. 58190, Morelia, Michoacán, Mexico.
E-mail addresses: karina_suarez@iim.unam.mx, karina.suarez.alcantara@gmail.com (K. Suárez-Alcántara).
http://dx.doi.org/10.1016/j.ijhydene.2016.06.242
0360-3199/

2Mg–Fe (i.e. formation of Mg_2FeH_6 after hydriding) [6–10]. ii) Fe addition from micrometric to nanometric powders size [11]. iii) Addition of Fe in order to form binary or ternary alloys with a wide range of metals and compositions [12–15]. iv) Addition of Fe as part of another compound such as Fe_2O_3, $FeTi_{1.2}$, $ZrFe_{1.4}Cr_{0.6}$ [2,16] or FeF_3 [17]. v) Addition of Fe in other systems such as Mg@Fe core–shell structures [18], graphite [19] or $LiBH_4/MgH_2$ reactive hydride composites [20]. Also, Fe is a common contaminant of the ball milling process when steel milling vials or balls are used [20–21]. Therefore Mg–Fe materials, in which the Fe source and content had been varied from just doping amounts to contents enough to form Mg_2FeH_6, appear as interesting and promising materials for hydrogen storage.

A large-scale production system of hydrogen storage materials must be efficient, cheap and environmentally friendly. An important weakness of any intended large-scale production system of hydrogen storage materials will be the high cost of preparation, handling, and storage under a high purity inert atmosphere. This weakness is common to all hydrogen storage materials based on metal hydrides that are sensible to oxygen and moisture. However; if large-scale utilization of hydrogen storage materials is envisioned, intentional or unintentional exposition to the air of materials might not be avoided at some point. Thus, it is highly advisable, to know a quick way to re-activate the materials and their hydriding/dehydriding response after such expositions. After exposition to air, it is expected the formation of MgO over the Mg surface. The formation of a MgO layer on the surface of Mg has been observed, theoretical and experimentally, to drastically decrease the diffusion of atomic hydrogen and to diminish the hydrogen storage capacity [22,23]. However, appropriate activation procedure could alleviate some of the adverse effects of the oxide formation in hydrogen storage materials [24]. Recently, Mg-LiH and Mg-M-LiH (M = Y, Zn, Al, Ag) alloys that were intentionally exposed to air demonstrated activity towards hydrogen storage [25]. In the present work, we study the production of Mg–Fe mixtures, their intentional exposition to air, an activation procedure, and the materials response to hydriding/dehydriding reactions.

Materials and methods

Materials preparation

Mg–Fe mixtures were prepared by ball milling in two different nominal proportions: 3 wt.% and 6 wt. % of Fe, respectively. Hereafter they will be referred to as Mg–Fe (3 wt.%) and Mg–Fe (6 wt.%). The raw metal powders of Fe and Mg (both 2.3 mm size, 99.8% purity, Alfa Aesar) were stored in an argon-filled glove box until mixture preparation. Each milling batch consisted of 30 g of metal powders and 3 mL of methanol as the milling control agent. The ball to powder ratio was 11:1. The milling vial and the balls were made of hardened steel. The milling vial, containing the powders, methanol, and balls, was tightly closed inside a glove box under high purity argon atmosphere. Then the vial was transferred to the mill located outside of the glove box. The milling process was performed in a planetary mill (Fritsch Pulverisette 6) at 350 rpm. The total effective milling time was 60 h in 40 cycles of 1.5 h of milling and 0.5 h of pause. After milling, the vial was cooled down to room temperature; then the lid of the vial was carefully loosened (so as to allow the influx of air) and the as-milled powders were exposed in this way to the air for 12 h. The whole milling procedure and air-exposure was settled accordingly previous experience of our research group [25]. As-milled powders were then collected and stored in argon atmosphere to avoid further oxidation. A sample of pure Mg powders was also milled and exposed to air for 12 h with the same procedure as the Mg–Fe mixtures. In the following, the characterization of the air-exposed Mg is presented for comparison whenever necessary.

Activation, hydriding/dehydriding cycling and Pressure-Composition-Temperature (PCT) data collection

Activation and hydrogen storage properties were performed on a carefully calibrated gravimetric equipment (PCTM-6000 Techno Systems Co., Ltd). Samples of 3 g of Mg, Mg–Fe (3 wt.%) and Mg–Fe (6 wt.%) were used for hydriding/dehydriding characterization. The weighing of each sample and transfer to the PCTM-6000 equipment was performed without atmosphere protection, i.e. in the open air. Once the sample was in place and sealed in the PCTM-6000, a pre-treatment or activation was performed consisting of vacuum pumping for 30 min at room temperature, followed by heating to a temperature of 350 °C (10 °C/min heating rate) while continuing vacuum pumping.

After reaching the 350 °C temperature, hydriding/dehydriding cycling was performed. Hydriding reactions were performed at 30 bar hydrogen pressure. Dehydriding reactions were performed by reducing the hydrogen pressure to 0.1 bar. The hydriding/dehydriding cycles were performed in a time-programmed way. For the hydriding reaction, the hydrogen pressure was increased from 0.1 bar to 30 bar over a period of 5 min and then the pressure was held at 30 bar for 55 min. The dehydriding reaction was carried out by decreasing the hydrogen pressure from 30 bar to 0.1 bar over a period of 5 min, then the pressure was held at 0.1 bar for 55 min. Three hydriding/dehydriding cycles were performed; the data shown in the Results section correspond to the 1st and the 3rd cycle. Following the cycles at 350 °C, the temperature was decreased to 300 °C and three cycles of hydriding/dehydriding were again performed. After that, a temperature of 250 °C was fixed and another three hydriding/dehydriding cycles were done. In case that the dehydriding reaction was not completed in the fixed time, particularly at 250 °C, the dehydriding was forced by heating up to 350 °C for 30 min, and then decreasing again the temperature to 250 °C. The sample of pure Mg powders was pre-treated in the same way as the Mg–Fe mixtures. However, the time-window of cycling was increased to 2.5 h for both the hydriding and the dehydriding reactions.

Pressure-Composition-Temperature (PCT) curves were determined at 350 °C and 300 °C using the same samples after performing the cycling tests described above. Each complete PCT curve data collection lasted about 1 week. The hydrogen pressure was gradually increased or reduced in a programmed way, provided a "stability" condition was achieved.

This stability condition is defined as no changes in the recorded weight in a selected number of measurements; in our experiments, this translated as no changes above 0.1 mg (3000 mg samples) in 60 measurements. One measurement was taken every 60 s. The sensibility of the balance of the gravimetric PCTM6000 system is 0.1 mg.

Finally, to perform the physical characterization of the hydrided materials, the samples were heated-up to 350 °C and exposed to 30 bar hydrogen pressure for 1 h. Then the system was cooled down to room temperature, the H_2 pressure was reduced then exchanged for Argon, and then the samples were transferred to an argon-filled glove box.

Physical characterization

The morphology of the as-prepared powder mixtures and the hydrided materials was observed in a scanning electron microscope (SEM, XL/SFEG/SIRION, FEI Company). Samples were dispersed on carbon tape and transferred to the SEM chamber. X-ray diffraction (XRD) experiments were performed on a SIEMENS D-500 diffractometer, using monochromatic $CuK_{\alpha 1}$ radiation ($\lambda = 1.54056$ Å). The XRD patterns were taken over the range from 20° to 80° in 2θ, with a step of 0.03° and 5 s per step. XRD patterns were analyzed with the help of the MAUD software and the crystal data available at the ICSD (Inorganic Crystal Structure Database- Karlsruhe) or at the COD (Crystallography Open Database). Rietveld analysis was performed with the MAUD Software over the whole experimental 2θ range.

Results

SEM and DRX characterization of as-milled and air-exposed materials

Fig. 1 presents the SEM image of as-milled Mg–Fe (3 wt.%). As-milled Mg and Mg–Fe (6 wt.%) SEM images are very similar to Fig. 1 and they are available in the Supplementary material. The ball-milling process produced Mg–Fe particles with sizes between 1 and 50 μm, with a majority of particles around 10 μm in size. The "popcorn-like" morphology was a common characteristic of Mg, Mg–Fe (3 wt.%) and Mg–Fe (6 wt.%) samples. The particle surfaces show features corresponding to stacked material, in agreement with the occurrence of cold-welding of particles during ball milling.

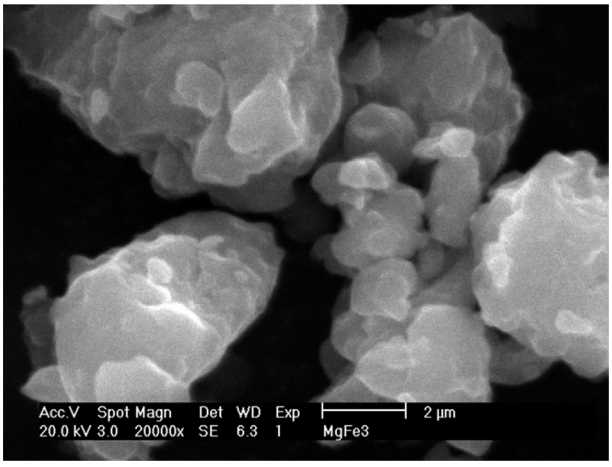

Fig. 1 – SEM micrographs of as-prepared materials of Mg–Fe (3 wt.%).

XRD patterns of the as-milled and air-exposed materials are presented in Fig. 2. The patterns exhibit the characteristic Mg and Fe peaks. Thus, the as-prepared materials consist of a fine mixture of Mg and Fe particles. Despite the expected formation of oxides after 12 h of air exposition, neither magnesium oxides nor iron oxides were evident from the XRD patterns. This is taken again in the Discussion section. Table 1 shows the results of calculations of lattice parameters and crystallite sizes. The Mg lattice was essentially unmodified by ball milling or the Fe addition. The crystallite size of Mg ranges between approximately 300 and 400 Å.

Activation and hydriding/dehydriding cycling results

Fig. 3 presents the first hydriding curve of Mg, Mg–Fe (3 wt.%) and Mg–Fe (6 wt.%) after the activation procedure; i.e. 30 min of vacuum pumping at room temperature, followed by heating to 350 °C while continuing vacuum pumping. As correspond to air-exposed materials, the hydrogen uptake is not completed in the programmed time, particularly at the air-exposed Mg. The Mg–Fe (6 wt.%) presented the best hydrogen uptake among the three samples, the numbers were: 2.5 wt.% for Mg; 4.2 wt.% for Mg–Fe (3 wt.%) and 5.1 wt.% for Mg–Fe (6 wt.%). Figs. 4–6 presents the third cycle of hydriding/dehydriding of the studied materials. The cycling led to the improvement of hydrogen uptake; this effect indeed alleviated in some degree the adverse effects of the air-exposure. Fig. 4 presents the hydriding/dehydriding cycling of Mg–Fe (3 wt.%) mixture at 350 °C, 300 °C and 250 °C. A maximum hydrogen uptake of 5.6 wt.% was achieved at

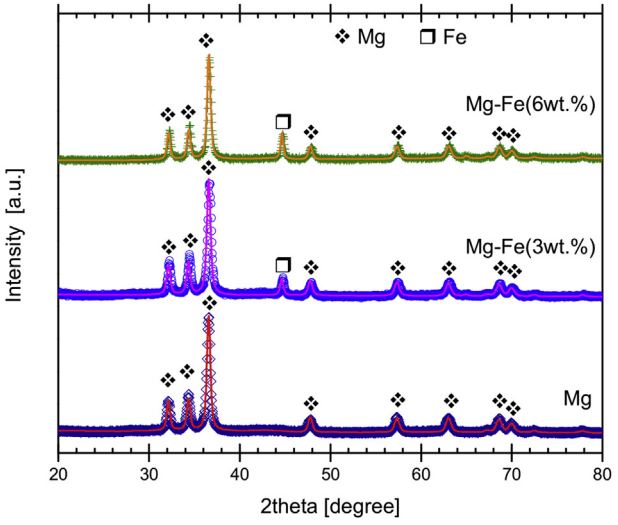

Fig. 2 – Powder X-ray diffraction patterns of as prepared (milled and air-exposed) Mg, Mg–Fe (3 wt.%) and Mg–Fe (6wt.%) mixtures. Dots: experimental data; line: Rietveld refined data.

Table 1 – Refined cell parameters and crystallite size of as-milled materials.

Material	Cell Parameters [Å] Mg (ICSD 642651): a = 3.20944 Å, c = 5.21076 Å Fe (ICSD 180969): a = 2.869 Å	Crystallite size [Å]
Mg	Mg: a = 3.212(4); c = 5.2153(5)	Mg: 355 ± 3
Mg–Fe (3 wt.%)	Mg: a = 3.212(2); c = 5.216(4) Fe: a = 2.869(3)	Mg: 299 ± 2 Fe: 354 ± 16
Mg–Fe (6 wt.%)	Mg: a = 3.203(1); c = 5.200(4) Fe: a = 2.862(2)	Mg: 407 ± 7 Fe: 1000 ± 59

350 °C. Released hydrogen accounted for 5.4 wt. % at 350 °C. Hydriding/dehydriding reactions were completed in 10 min at this temperature. At 300 °C, the hydrogen uptake was finished in 30 min reaching 5.4 wt.%; meanwhile, the dehydriding reaction was slower, achieving only 4.8 wt.% of released hydrogen in 50 min. The hydriding/dehydriding reactions at 250 °C were not completed in the programmed time. The hydrogen uptake was 4.8 wt.%, while only 1.1 wt. % hydrogen was desorbed (both measurements made in one hour time). The amount of hydrogen uptake/release and the hydriding kinetics correspond well with the temperature, i.e. at higher temperature, faster kinetics and larger hydrogen uptake.

Fig. 5 presents the hydriding and dehydriding cycles for the Mg–Fe (6 wt.%) mixture. In this mixture, the maximum hydrogen uptake was 6.2 wt. % at 350 °C. This is slightly higher than the hydrogen uptake observed in Mg–Fe (3 wt.%) at the same temperature. The maximum hydrogen uptake at 300 °C was 5.8 wt.%. Hydriding reactions were mostly completed in 10 min at 350 °C and 300 °C. At 250 °C, the hydrogen uptake was 5.0 wt.% and the kinetics was remarkable slower compared with the experiments at higher temperatures. Other observed effects of the larger Fe addition were an improvement of the dehydriding kinetics and an increase in the total amount of released hydrogen. At 350 °C and 300 °C the fast stage of the hydriding reaction lasted for about 10 min; at 250 °C, it was about 30 min. The dehydriding reaction was well completed at 350 °C and 300 °C, while during 1 h dehydriding at 250 °C, the Mg–Fe (6 wt.%) mixture released 2.9 wt. % H_2.

Fig. 6 presents the hydriding/dehydriding cycles of air-exposed Mg powders. Hydrogen uptake at 350 °C was about 5.4 wt.% after 2.5 h reaction. The dehydriding reaction was slow; it was completed after 1 h reaction. The hydriding reaction at 300 °C followed practically the same kinetics than at 350 °C; however, dehydriding was not completed within the 2.5 h test time (only about 1 wt.% hydrogen was released). No hydriding/dehydriding reactions were observed for the air-exposed Mg powders at 250 °C. Thus, a clear beneficial effect of Fe addition was found. Table 2 summarizes the data on hydrogen uptake for Mg–Fe and Mg powders.

Pressure-Composition-Temperature (PCT) data collection

Figs. 7 and 8 present the PCT curves of Mg–Fe (3 wt.%) and Mg–Fe (6 wt.%) mixtures at 350 °C and 300 °C respectively. The hydrogen uptake and release values were the same as obtained in the hydriding and dehydriding cycle reactions. PCT curves at Figs. 7 and 8 demonstrate that the hydrogen release can be possible at 1 bar although in the present work 0.1 bar hydrogen pressure was used at the cycling experiments. In a related study of air-exposed Mg–Li alloys of our research group [25], PCT curve of air-exposed Mg at 350 °C showed a

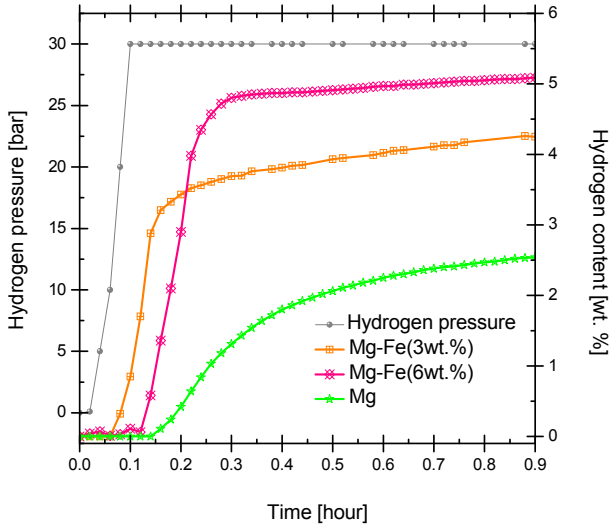

Fig. 3 – First hydriding curve of air-exposed Mg, Mg–Fe (3 wt.%) and Mg–Fe (6 wt.%) materials at 350 °C and 30 bar.

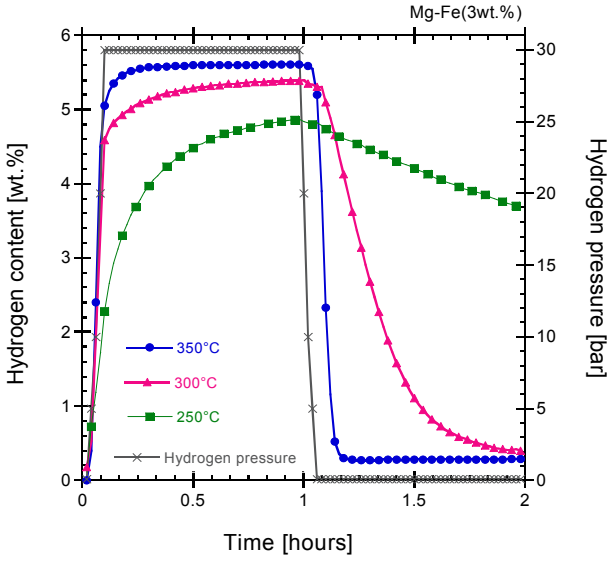

Fig. 4 – Hydriding/dehydriding cycles of the Mg–Fe (3 wt.%) mixture (ball milled and air-exposed). Hydriding at 30 bar, dehydriding at 0.1 bar.

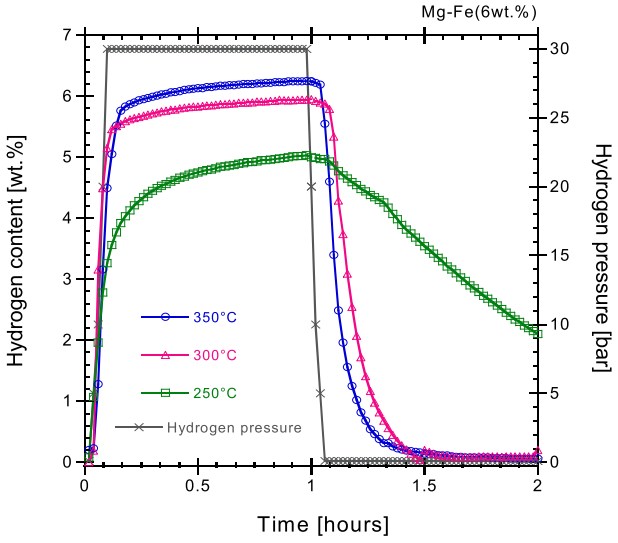

Fig. 5 – Hydriding/dehydriding cycles of the Mg–Fe (6 wt.%) mixture (ball milled and air-exposed). Hydriding at 30 bar, dehydriding at 0.1 bar.

huge hysteresis between the hydriding and dehydriding equilibrium pressures: 17 bar for hydriding and 0.7 bar for dehydriding. At the Mg–Fe (3 wt.%) and Mg–Fe (6 wt.%) mixtures, there was an appreciable hysteresis between hydriding and dehydriding equilibrium pressures. However, PCT graphics of Figs. 7 and 8 show that the hysteresis was appreciably reduced by the Fe incorporation, compared to Mg [25]. The equilibrium pressures are at 350 °C: 8.5 bar for hydriding and 2.5 bar for dehydriding at the Mg–Fe (3 wt.%) mixture and 9.0 bar for hydriding and 3.5 bar for dehydriding at Mg–Fe (6 wt.%) mixture.

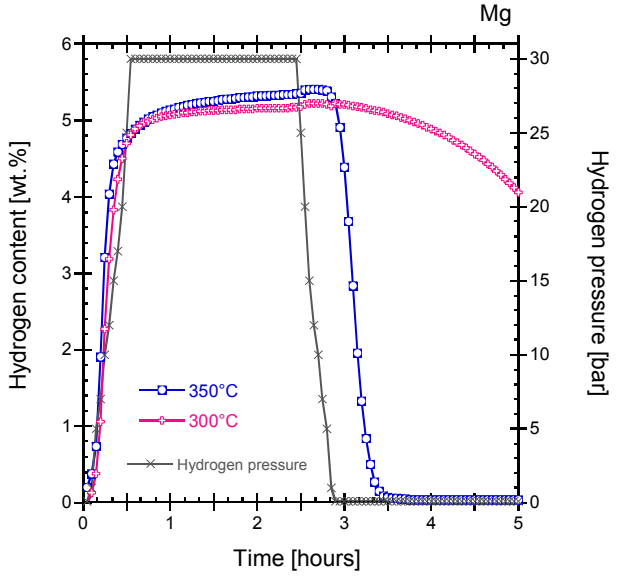

Fig. 6 – Hydriding/dehydriding cycles of the Mg (ball milled and air-exposed). Hydriding at 30 bar, dehydriding at 0.1 bar.

Table 2 – Hydrogen uptake/release data of air-exposed Mg, Mg–Fe (3 wt.%) and Mg–Fe (6 wt.%).

Material	Hydrogen uptake [wt.%]	Hydrogen release [wt.%]
Mg	250 °C: No reaction	250 °C: No reaction
	300 °C: 5.0 (24.0 min[a])	300 °C: 1.0 (60 min[b])
	350 °C: 5.4 (19.8 min[a])	350 °C: 5.4 (45.6 min[a])
Mg–Fe (3 wt.%)	250 °C: 4.8 (16 min[a])	250 °C: 1.1 (60 min[b])
	300 °C: 5.4 (6.0 min[a])	300 °C: 5.0 (30 min[a])
	350 °C: 5.6 (4.8 min[a])	350 °C: 5.3 (7.2 min[a])
Mg–Fe (6 wt.%)	250 °C: 5.0 (10.8 min[a])	250 °C: 2.9 (60 min[b])
	300 °C: 5.8 (5.4 min[a])	300 °C: 5.8 (15.6 min[a])
	350 °C: 6.2 (7.2 min[a])	350 °C: 6.2 (10.8 min[a])

[a] α = 0.8 completed within the experimental time; value in parenthesis.
[b] α = 0.8 not completed within the experimental time; value read at 60 min of experiment.
α is the transformed fraction, i.e. the ratio between the hydrogen uptake at any time and the final hydrogen uptake.

Although only two PCT experiments at different temperatures (350 °C and 300 °C) were performed on the studied Mg–Fe mixtures, the reaction enthalpy and entropy was obtained with the van't Hoff relationship [26]:

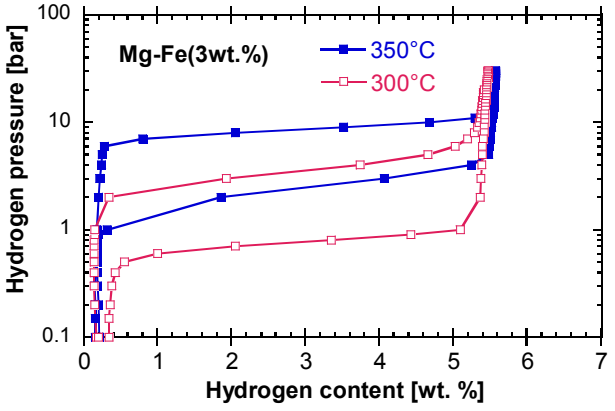

Fig. 7 – PCT diagram of Mg–Fe (3 wt.%) mixture, all data experimental shown.

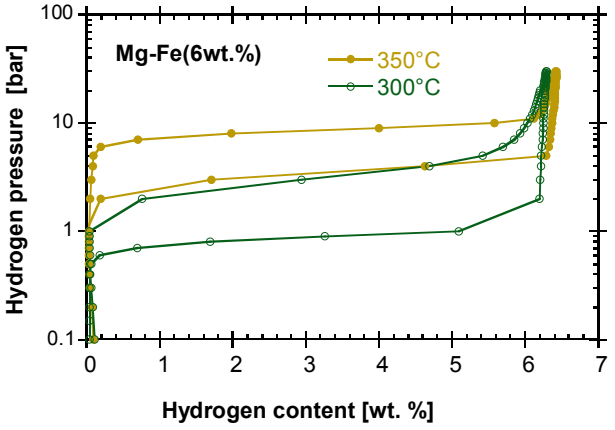

Fig. 8 – PCT diagram of Mg–Fe (6 wt.%) mixture, all data experimental shown.

$$\ln\left(p_{H_2}\right) = \frac{\Delta H}{RT} - \frac{\Delta S}{R}. \quad (1)$$

The enthalpy and entropy values were basically the same for both Mg–Fe mixtures. For the hydriding reactions, the values: $\Delta H_{abs} = -62$ kJ mol^{-1} H_2 and $\Delta S_{abs} = -117$ J K^{-1} mol^{-1} H_2 were obtained. For the dehydriding reactions the values were: $\Delta H_{des} = -74$ kJ mol^{-1} H_2 and $\Delta S_{des} = -130$ J K^{-1} mol^{-1} H_2. The enthalpy and entropy values are consistent with values reported for Mg/MgH_2 system [26]. These data indicate rather a kinetic effect than a thermodynamic effect by the addition of Fe to Mg.

SEM and DRX characterization of hydrided materials results

Fig. 9 presents the SEM image of hydrided Mg–Fe (3 wt.%). Interestingly, the formation of globular nodules all over the particle surface was observed. After heat pre-treatment and hydriding/dehydriding cycles, particle sizes do not experiment significant changes. The particle size ranged between 1 and 50 μm, with a large number of particles around 10 μm size. SEM images of hydrided Mg and Mg–Fe (6 wt.%) are similar to Mg–Fe (3 wt.%) SEM images and can be found in the Supplementary material.

Fig. 10 presents the XRD patterns of hydrided materials; the main phases are MgH_2, unreacted Mg, Fe and MgO. This result suggests that MgO was formed after the 12-h of air exposition as an amorphous layer over the Mg–Fe particles and, that only after heat treatment the MgO crystalized and become evident at RXD experiments. Table 3 presents the relevant Rietveld-refined data of hydrided materials. Cell lattices of MgH_2, MgO and Fe were not presented in Table 3; their values were in agreement with the reported data at ICSD or COD crystallographic databases. Thus, no changes in the crystallographic parameters were generated by heat activation and hydriding/dehydriding reactions. On the other hand, MgO content seems to have a direct relationship to the Fe addition level. MgO content was reduced from 31.8 wt.% to 12.5 wt.% by the addition of 6 wt.% Fe.

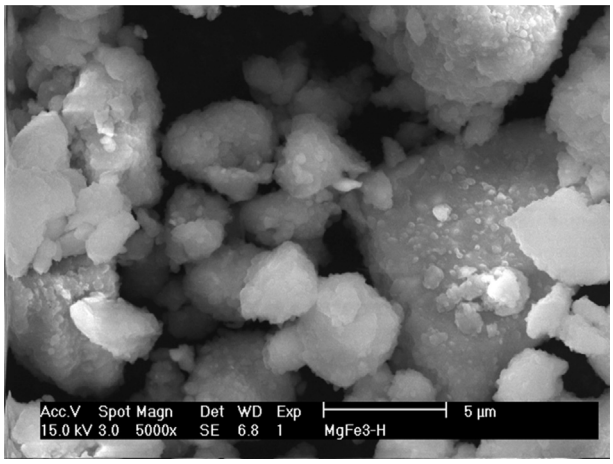

Fig. 9 – SEM micrographs of hydrogenated Mg–Fe (3 wt.%).

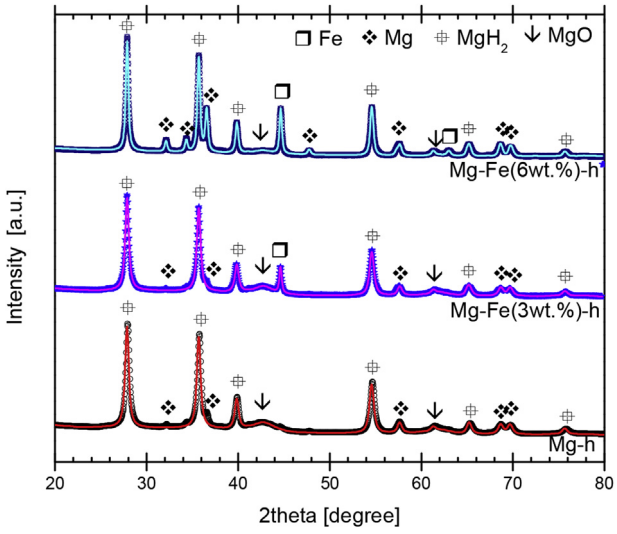

Fig. 10 – Powder X-ray diffraction patterns of hydrogenated Mg, Mg–Fe (3 wt.%) and Mg–Fe (6 wt.%) mixtures. Dots: experimental data; line: Rietveld refined data.

Discussion

The Fe catalyst and the activation effects

Antisari et al., in a study of a MgH_2–Fe material, suggested that Mg nucleation sites are constituted of structural defects at grain boundaries; and that ball milling and the addition of Fe increase the number of nucleation sites [27]. The intensive ball-milling time was performed to ensure the homogeneous distribution of the Fe and the creation of a considerable number of structural and surface defects. After the air-exposure, MgO formation was expected to block a huge fraction of nucleation or active sites. After the pre-treatment, i.e. heating in vacuum, it was demonstrated that many of the active sites were still suitable for inducing hydrogen storage (Fig. 3). Nonetheless, the main activation procedure was the hydride/dehydriding cycling (Fig. 4). The effects of Fe addition to Mg were an increase of the hydrogen uptake, hydrogen release, and in general, an improvement of hydriding/dehydriding kinetics. Another interesting Fe effect was that the addition of 6 wt.% of Fe demonstrated a reduced formation of crystalline MgO and an increased hydrogen uptake. Hydriding/dehydriding and PCT curves clearly demonstrated a positive effect of Fe in increasing the hydrogen uptake/release and reducing the hysteresis between the hydriding/dehydriding pathways. Similar results on hydrogen uptake have been reported for Mg materials that were carefully protected against air exposition [2,6–21,28]. Thus, air-exposure could not be as critical as believed for hydrogen uptake on Fe–Mg mixtures.

The air exposition effect

After the air exposition of Mg particles, it is always expected the formation of an oxide layer. The major negative effects of the MgO layer have been recognized as the reduction of the hydrogen uptake capacity and slowing the hydriding/dehydriding kinetics [29]. In the studied materials, only after heat

Table 3 – Rietveld analysis of hydrogenated materials and the expected hydrogen storage capacity.

Material	MgO content [wt.%]	Expected H_2 storage capacity [wt.%][a]	MgO crystal size [Å]	MgH_2 crystal size [Å]	Fe crystal size [Å]
Mg	31.8 ± 0.4	5.2	36.5 ± 0.6	251.3 ± 0.8	–
Mg–Fe (3 wt.%)	23.5 ± 0.4	5.6	47.6 ± 0.9	252.6 ± 0.9	603.0 ± 17
Mg–Fe (6 wt.%)	12.5 ± 0.4	6.2	44.3 ± 1.8	419.5 ± 2.3	630.1 ± 11

[a] (100-wt.%MgO-wt.%Fe)*7.6/100.

activation, hydriding/dehydriding cycles and PCT data collection, it was observed the crystallization of that layer. The kinetics of the MgO growing over Mg or MgH_2 is well-known [30–33]. For the MgO layer growing over Mg, it consists of three stages; i) oxygen chemisorption, ii) oxide nucleation and island growth, and iii) coalescence of the oxide islands [30]. Do et al. also proposed that the oxide layer rapidly grows up to some critical thickness and then stops. The critical thickness is dependent on a critical temperature, above which the oxide growth continues without limit [30]. Do et al. estimated the critical thickness of MgO over Mg + Air as 2.55 nm, although no clear reference to the critical temperature was given. Meanwhile, McIntyre et al. [33], suggested that an oxide thickness of about 2.2 nm can be formed even at 10 s of ambient exposure and that the oxide thickness continued increasing with the time of exposition. The data presented reached up to 10 months and 4.5 nm thickness [33]. Accordingly to the data presented by McIntyre et al. [33], and based on the exposure time of 12 h, the Mg oxide film thickness would be about 3 nm. Do and McIntyre thickness estimations do not match with the high percentage of MgO obtained by our Rietveld analysis; which in turn is indeed consistent with the kinetics and PCT curves, i.e. the proportion of MgO and MgH_2 formed (Table 3). Based just on geometry and density of materials; a Mg spherical particle of 10 μm diameter covered by a MgO 500–800 nm layer will give a MgO content about 17–29 wt.%, which is in the range of the values presented in Table 3. SEM images after hydriding of materials (Fig. 9) demonstrated the formation of globular nodules or protuberances at the particle surface. Although it is difficult to assign based solely on SEM images, it is possible that these protuberances correspond to coalesced MgO, formed in turn by MgO nano-crystal of about 35–50 Å (3.5–5.0 nm, Table 3). MgO cracks, fissures or incomplete coverage of Mg/MgH_2 can lead to hydrogen reaching clean surfaces as a result of the pre-treatment and cycling, i.e. the whole activation process. At our samples, still with the negative effects of the MgO formation, the hydrogen uptake reached a maximum of 6.2 wt.% of stored hydrogen. The 6.2 wt.% of hydrogen uptake (350 °C and 30 bar) of our air-exposed materials is comparable to a recent report of a Mg–Fe material (5 wt.% Fe) [34], where the sample was carefully protected by argon atmosphere and the hydrogen uptake was 7 wt.% (375 °C and 80 bar). Thus, it was demonstrated the feasibility of hydrogen storage after an air exposition event. However, an important delay in the time for completing hydriding and dehydriding reactions was observed as compared with carefully protected materials, where the same reactions can be completed even in less than 100 s [2,6–21,28,34].

Conclusions

Mg–Fe (3 wt.%) and Mg–Fe (6 wt.%) mixtures were prepared by ball milling, exposed to air for 12 h and tested for hydrogen storage capabilities. It was demonstrated that between 5.6 wt.% and 6.2 wt.% of hydrogen storage is feasible in an experimental range of 250°C–350 °C at the air-exposed Mg–Fe mixtures. Fe proved to be an effective catalyst to improve the hydriding/dehydriding reactions for the air-exposed materials. The MgO formation by air exposition was not, after all, a critical factor that impedes the hydriding/dehydriding reactions if proper activation is carried out. However, an important delay in the time for completing hydriding/dehydriding reaction is recognized.

Acknowledgments

The present work was supported by the UNAM-DGAPA-PAPIIT IA100415.

Appendix A. Supplementary data

Supplementary data related to this article can be found at http://dx.doi.org/10.1016/j.ijhydene.2016.06.242.

REFERENCES

[1] Jia Y, Sun C, Shen S, Zou J, Mao SS, Yao X. Combination of nanosizing and interfacial effect: future perspective for designing Mg-based nanomaterials for hydrogen storage. Renew Sustain Energy Rev 2015;44:289–303.
[2] Sakintuna B, Lamari-Darkrim F, Hirscher M. Metal hydride materials for solid hydrogen storage: a review. Int J Hydrogen Energy 2007;32:1121–40.
[3] Schlapbach L, Züttel A. Hydrogen-storage materials for mobile applications. Nature 2001;414:353–8.
[4] Bououdina M, Grant D, Walker G. Review on hydrogen absorbing materials structure, microstructure, and thermodynamic properties. Int J Hydrogen Energy 2006;31:177–82.
[5] Felderhoff M, Bogdanović B. High temperature metal hydrides as heat storage materials for solar and related applications. Int J Mol Sci 2009;10:325–44.
[6] Bassetti A, Bonetti E, Pasquini L, Montone A, Grbovic J, Vottori Antisari M. Hydrogen desorption from ball milled MgH_2 catalyzed with Fe. Eur Phys J B 2005;43:19–27.

[7] Zhou DW, Li SL, Varin RA, Peng P, Liu JS, Yamg F. Mechanical alloying and electronic simulations of Mg-Fe mixture powders for hydrogen storage. Mater Sci Eng A 2006;427:306–15.
[8] Liang G, Hout J, Boily S, Van Neste A, Schulz R. Catalytic effect of transition metals on hydrogen sorption in nanocrystalline ball milled MgH_2-Tm (Tm=Ti, V, Mn, Fe, Ni) systems. J Alloys Compd 1999;292:247–52.
[9] Bogdanovic B, Reiser A, Schlichte K, Spliethoff B, Teche B. Thermodynamics and dynamics of the Mg-Fe-H system and its potential for thermochemical thermal energy storage. J Alloys Compd 2002;345:77–89.
[10] Pozzo M, Alfe D. Hydrogen dissociation and diffusion on transition metal (= Ti, Zr, V, Fe, Ru, Co, Rh, Ni, Pd, Cu, Ag)-doped Mg(0001) surfaces. Int J Hydrogen energy 1922-1930;2009:34.
[11] Hanada N, Ichikawa T, Fujii H. Catalytic effect of nanoparticle 3d-transition metals on hydrogen storage properties in magnesium hydride MgH_2 prepared by mechanical milling. J Phys Chem B 2005;109:7188–94.
[12] Youp Song M, Baek SH, Bobet JL, Hong SH. Hydrogen storage properties of a Mg-Ni-Fe mixture prepared via planetary ball milling in a H_2 atmosphere. Int J Hydrogen Energy 2010;35:10366–72.
[13] Kwon SN, Baek SH, Mumm DR, Hong SH, Song MY. Enhancement of the hydrogen storage characteristics of Mg reactive mechanical grinding with Ni, Fe and Ti. Int J Hydrogen Energy 2008;33:4586–92.
[14] Kalisvaart WP, Harrower CT, Haagsma J, Zahiri B, Luber EJ, Ophus C, et al. Hydrogen storage in binary and ternary Mg-based alloys: a comprehensive experimental study. Int J Hydrogen Energy 2010;35:2091–103.
[15] Zahiri B, Harrower CT, Amirkhiz BS, Mitlin D. Rapid and reversible hydrogen sorption in Mg-Fe-Ti thin films. Appl Phys Lett 2009;95:103114–103114-3.
[16] Jung KS, Lee EY, Lee KS. Catalytic effects of metal oxide on hydrogen absorption of magnesium metal hydride. J Alloys Compd 2006;421:179–84.
[17] Yavari AR, LeMoulec A, de Castro FR, Deledda S, Friedrichs O, Botta WJ, et al. Improvement in H-sorption kinetics od MgH_2 powders by using Fe nanoparticles generated by reactive FeF_3 addition. Scr Mater 2005;52:719–24.
[18] Zou J, Long S, Zhang L, Lu C, Chen X, Zeng X, et al. Hydrogen sorption behaviors of a core-shell structured Mg@Fe composite powder. Mater Trans 2014;55:1156–60.
[19] Isobe S, Ichikawa T, Gottwald JI, Gomibuchi E, Fujii H. Catalytic effect of 3d transition metals on hydrogen storage properties in mechanically milled graphite. J Phys Chem Solids 2004;65:535–9.
[20] Puszkiel JA, Gennari FC, Arneodo Larochette P, Ramallo-Lopez JM, Vainio U, Karimi F, et al. Effect of Fe additive on the hydriding-dehydriding properties of $2LiH + MgB_2/2LiBH_4 + MgH_2$ system. J Power Sources 2015;284:606–16.
[21] Baum L, Meyer M, Mendoza-Zélis L. Hydrogen storage properties of the Mg/Fe system. Physica B 2007;389:189–92.
[22] Wu G, Zhang J, Wu Y, Li Q, Chou K, Bao X. Adsorption and dissociation of hydrogen on MgO surface: a first-principles study. J Alloys Compd 2009;480:788–93.
[23] Ostenfeld CW, Johansson M, Chorkendorff I. Hydriding properties of catalyzed and non-catalyzed magnesium films. Surf Sci 2007;601:1862–9.
[24] Manchester FD, Khatamian D. Mechanisms for activation of intermetallic hydrogen absorbers. Mater Sci Forum 1988;31:261–96.
[25] Suárez-Alcántara K, Palacios-Lazcano AF, Funatsu T, Cabañas-Moreno JG. Mg-M-LiH alloys prepared by mechanical milling and their hydrogen storage characteristics. Int J Hydrogen Energy 2015;40:17344–53.
[26] Bogdanovic B, Bohmhammel K, Christ B, Reiser A, Schlichte K, Vehlen R, et al. Thermodynamic investigation of the magnesium–hydrogen system. J Alloys Compd 1999;282:84–92.
[27] Vittori Antisari M, Aurora A, Mirabile Gattia D, Montone A. On the nucleation step in the $Mg–MgH_2$ phase transformation. Scr Mater 2009;61:1064–7.
[28] Amirkhiz BS, Zahiri B, Kalisvaart P, Mitlin D. Synergy of elemental Fe and Ti promoting low temperature hydrogen sorption cycling of magnesium. Int J Hydrogen Energy 2011;36:6711–22.
[29] Jensen TR, Andreasen A, Vegge T, Andreasen JW, Stahl K, Pedersen AS, et al. Dehydriding kinetics of pure and nickel-doped magnesium hydride investigated by in situ time-resolved powder X-ray diffraction. Int J Hydrogen Energy 2006;31:2052–62.
[30] Do T, Splinter SJ, Chen C, McIntyre NS. Measurement of oxide film growth on Mg and A1 surfaces over extended periods using XPS. Surf Sci 1997;387:192–8.
[31] Chen C, Splinter SJ, Do T, Mclntyre NS. The oxidation kinetics of Mg and A1 surfaces studied by AES and XPS. Surf Sci 1997;382:L652–7.
[32] Friedrichs O, Sanchez-Lopez JC, Lopez-Cartes C, Dornheim M, Klassen T, Bormann R, et al. Chemical and microstructural study of the oxygen passivation behavior of nanocrystaline Mg and MgH_2. Appl Surf Sci 2006;252:2334–45.
[33] McIntyre NS, Chen C. Role of impurities on Mg surfaces under ambient exposure conditions. Corros Sci 1998;40:1697–709.
[34] Chun C, Ai-Min Y. High-temperature hydrogen cycling properties of magnesium-based composites. Mater Lett 2016;169:144–7.